Available online at www.sciencedirect.com
ScienceDirect
Applied Thermal Engineering 27 (2007) 1009–1016
Applied Thermal Engineering
www.elsevier.com/locate/apthermeng

Isothermal composite adsorbent. Part I: Thermal characterisation

L. Meljac, V. Goetz *, X. Py

PROMES-CNRS UPR 8521, Université de Perpignan UPVD, Tecnosud, Rambla de la Thermodynamique, 66100 Perpignan, France

Received 21 December 2005; accepted 18 July 2006
Available online 18 October 2006

Abstract

Adsorption and desorption are respectively exo and endothermic phenomena leading to significant temperature changes in adsorption columns. Enhanced efficiency of a sorption process could be obtained under isothermal conditions, either for gas storage, purification or separation applications. The heat transfer within the adsorbent beds can be managed in situ, using thermal energy storage material: a phase change materials (PCM) for example. The thermal behaviour of a mixture of activated carbon and PCM during CO_2 adsorption has been studied. The thermal characteristics of the involved materials have been determined and experiments carried out to highlight the positive effect of the PCM to reduce the CO_2 adsorption heat effects on an activated carbon bed. Calorimetry was the technique used for all the thermal characterisations. It appears that the heat effects induced by CO_2 adsorption are reduced by the presence of the PCM together with the adsorbent. The endothermic effect of fusion balances the heat effect of adsorption and significantly reduces the temperature changes.

Keywords: Calorimetry; Adsorption; PCM; Thermal effect

1. Introduction

The adsorptive properties of microporous solid are currently used in numerous industrial applications such as air purification, drinking water, gas separation or gas storage. These processes are operated under different thermodynamic conditions: temperatures, pressures and gas flowrates to be treated. Their performances are closely linked to the choice of a microporous solid well-suited to the process working conditions but also to the heat and mass transfer conditions inside the columns. This last point is often a limitation to the performances of the processes in dynamical conditions. As an example, in the case of natural gas storage system based on adsorption, the dynamic efficiency of the unit is highly dependent on the heat conductivity of the packing adsorbent [1,2]. In the same way, an efficient management of the heat powers produced or needed during the successive adsorption/desorption phases involved in pressure swing adsorption processes, should lead to an increase of the level of performance in terms of selectivity and storage capacity of the column [3–5]. Therefore, it can be considered that, on a general point of view, isothermal sorption conditions correspond to the best operating-mode of sorption processes leading to optimal performance.

Few solutions were proposed to reduce or manage the thermal effects generated during adsorption/desorption of gas species on microporous adsorbent. Basically, two different approaches can be considered. The first one is the extraction from the column (or the supply to the column) of the heat fluxes generated by adsorption (or desorption). In this case, the implementation of a heat exchanger is needed at the external surface of the adsorption column and packing adsorbents must present high level of heat conductivity as well as high heat exchange coefficient with the surface of the column. Expanded natural graphite associated with adsorbent has already demonstrated its efficiency as thermal binder [6]. Nevertheless, this way of heat management is limited to columns with small diameter and can hardly be extended to industrial applications

* Corresponding author. Tel.: +33 4 68 68 22 36; fax: +33 4 68 68 22 13.
E-mail address: goetz@univ-perp.fr (V. Goetz).

1359-4311/$ - see front matter © 2006 Elsevier Ltd. All rights reserved.
doi:10.1016/j.applthermaleng.2006.07.037

where the columns and the mass flows to be treated are very large.

The second possibility is a local management of the heat fluxes at the scale of the grain or the pellet of adsorbent where the heat effects are produced by the adsorption or desorption of the species. To achieve such an internal thermal management, we have tested a new kind of composite material [7] made of grains of adsorbent and liquid/solid phase change materials (PCM) that can store large amount of heat in almost isothermal conditions. These composites should be particularly adapted for PSA processes involving successive adsorption/desorption steps. In the case of gas storage, previous attempt of association of adsorbent with PCMs were already tested. Nevertheless, direct impregnation of the PCM within the porosity of the adsorbent leads to high interaction with the adsorption phenomenon leading to a drastic decrease of the adsorption efficiency and a modification of the phase change properties of the PCM [8]. In the present paper, the selected approach consists in the association of micro-encapsulated phase change materials (μ-PCMs) with adsorbent grains. Today, μ-PCMs are produced industrially by different manufacturers. They were initially developed more specifically for textile applications [9–11] but have been also tested more recently for heat management in building [12,13].

In the present study, the thermal behaviour of a mixture of μ-PCMs and adsorbent during gas adsorption has been studied. Experimental methods based on calorimetry were developed in order to demonstrate the efficiency of this mixture to manage the thermal effect during adsorption.

2. Materials and method

2.1. Materials

The studied composite is made of RB2 granules of activated carbon (AC), supplied by NORIT Co., and of μ-PCM Ceracap NB 1005 X manufactured by BASF. The two components were simply physically mixed together.

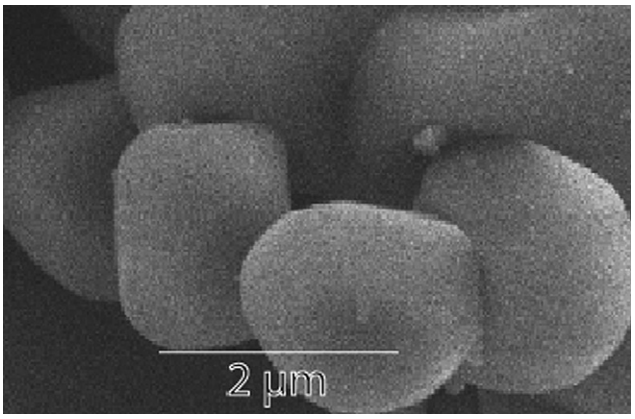

Fig. 1. SEM picture of PCM nodules.

The studied PCM is a paraffin oil with a melting point of 35 °C and industrially μ-encapsulated in a melamine resin membrane by a polycondensation process. The diameter of the nodules varies from 1.5 μm to few μm (Fig. 1).

2.2. Calorimetry

Calorimetry was the method used for all the thermal analysis carried out in this study. The experimental set up is shown in Fig. 2.

The calorimeter was a C80 from SETARAM Company. It was equipped with two high pressure cells, which could stand temperature up to 300 °C and a pressure up to 100 bars. The sample was placed in the working cell while the other cell was remained empty. As the reference cell was set perfectly symmetrical to the working one, the signal delivered by the calorimeter corresponds exactly to the thermal effect generated in the working cell.

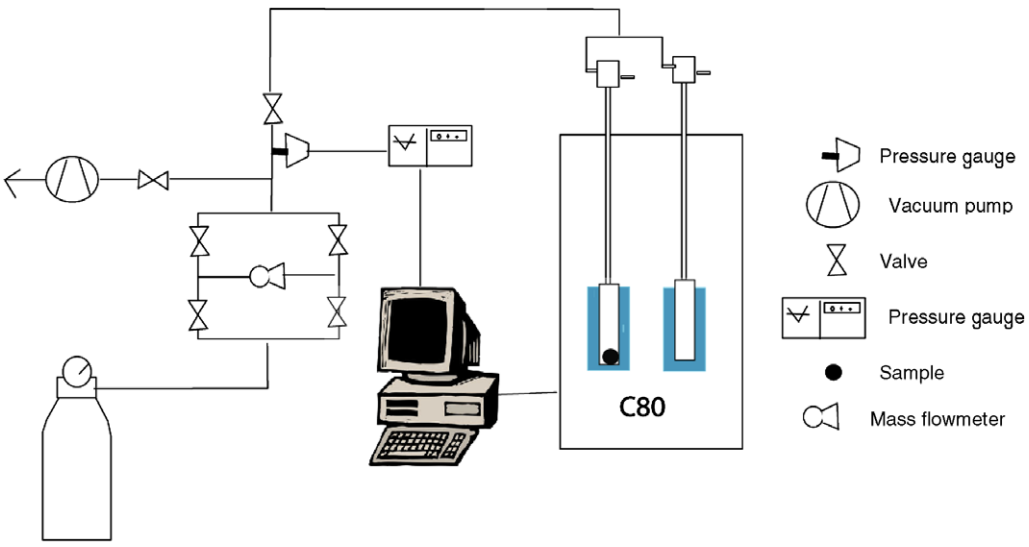

Fig. 2. Experimental set up.

The cells were surrounded by two fluxmeters each of which is a bundle of hundred of thermocouples. The fluxmeters detected the whole thermal power generated in the cells regardless the sample disposition or geometry [14,15].

The heat flow, the temperature inside the calorimeter vessel and the pressure in the cells were recorded by a software and plotted versus time. The enthalpy variations in the working cell were calculated by the integration of the measured heat flow signals [16,17].

Using this experimental set up, it is possible to operate under isothermal conditions and to set a constant heating rate of the cells. Moreover, a controlled increase in pressure using the mass flow controller can also be realised, as well as pressure steps by opening all the valves that connect the cells to the CO_2 storage vessel. For pressure steps, the pressure inside the cells is controlled by a pressure reducer.

Throughout the experiments, the pressure was ranged from 0 to 11.3 bars, and the temperature from 24 to 50 °C.

Before any experiments, the RB2 adsorbent was out gassed under deep vacuum at 100 °C for 24 h. Then, it was introduced in the calorimeter cell and out gassed once more, under primary vacuum at 100 °C for 2 h, to remove any remaining water that could potentially be adsorbed by the activated carbon during its transfer into the calorimeter cell.

3. Experimental results

In the first set of experiments, RB2 and μ-PCM were treated separately in order to measure some of their intrinsic thermal characteristics. Each experiment was carried out several times to ensure their accuracy and check their reproducibility.

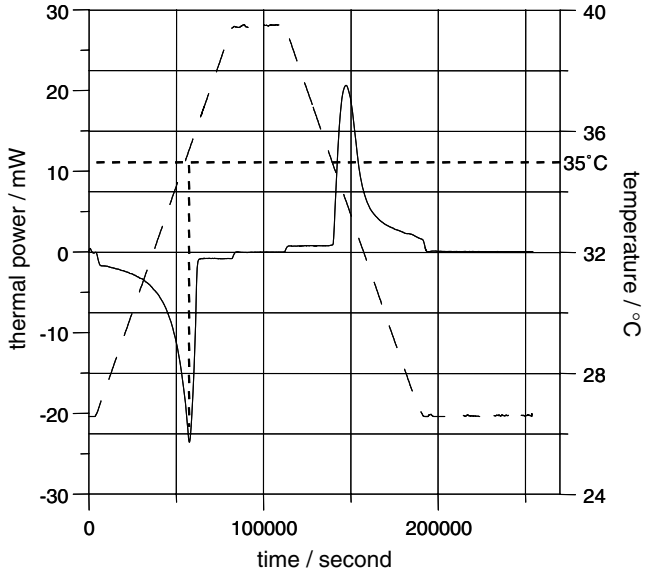

Fig. 3. Determination of C_p and ΔH_{fusion} of PCM, (—) thermal power, (----) temperature.

3.1. Sensible and latent heat of PCM phase change

A μ-PCM loading of 2.49 g was introduced into the calorimeter working cell and exposed to a temperature cycle between 26.5 and 39.5 °C under inert atmosphere (1 bar of nitrogen). The obtained calorimeter signal is plotted in Fig. 3.

In order to set the calorimeter to a stable baseline, the temperature was initially kept constant. During the heating ramp and as soon as the temperature started to be increased an endothermic effect was detected. The corresponding heat flux decreased very quickly until the temperature reached 35 °C, which corresponds to the end of the PCM phase change. This endothermic effect was due to the PCM melting process. Once the PCM was completely in the liquid state, the phase change endothermic effect stopped and the working cell recovered the constant rate temperature increase. At this stage, as the μ-PCM sensible heat was the only contribution to the endothermic effect, the heat flux generated by the working cell became constant. Finally, the calorimetric signal recovered the baseline when the temperature rise was over. During the cooling step, an exothermic effect was first detected, due to the heat capacity of the μ-PCM. It remained constant until 35 °C was reached. From this temperature level, the dissipated heat flux increased sharply due to the PCM solidification, before decreasing slowly until the whole thermal cycle was achieved.

According to the tails observed on the two peaks (below and above 35 °C under melting and solidification, respectively), one can conclude that the PCM is not composed of a unique species but is made of a mixture of paraffin chains among which the heaviest melts at 35 °C. This is the reason why the two calorimetric signals present asymmetric characters with respect to the melting temperature of 35 °C with a tail observed in both cases within the lowest temperature range.

At constant heating rate, sensible heat induces a constant heat fluxes. Therefore, the plateau reached after melting and before solidification of the PCM can be related to the melted μ-PCM heat capacity by the following equation:

$$C_{p\text{PCM}} = \frac{W}{m_{\text{PCM}} \cdot \frac{dT}{dt}}, \tag{1}$$

where W refers to the measured thermal power and m_{PCM} to the μ-PCM load.

Under controlled heating rate, C_p can be estimated from Eq. (1). This led to the following result:

$$C_{p\text{PCM}} = 1.9\ \text{kJ kg}^{-1}\ \text{K}^{-1} \pm 5\% \tag{2}$$

This value has been confirmed using several measurements made on several samples of μ-PCM. The heat capacity of the μ-PCM in the solid state cannot be efficiently calculated because the temperature at which the whole PCM is in solid state could not be easily reached with the involved equipment.

According to the literature, the heat capacity of paraffin oils is around 2.2 kJ kg^{-1} K^{-1} [18]. The difference between this value and our experimental one can be explained by the contribution of the melamine resin (0.07 kJ kg^{-1} K^{-1}) that encapsulates the paraffin oil the heat capacity of which is smaller than that of the PCM.

Tacking into account the simultaneous contributions of the sensible and latent heats, the integration of the first or second peak of the Fig. 3, allowed us to calculate the latent heat of the PCM phase change:

$$\Delta H_{\text{fusion}} = \frac{\Delta H}{m_{\text{PCM}}} - C_{p\text{PCM}} \cdot \Delta T, \tag{3}$$

where ΔH corresponds to the total heat obtained from the peak curve integration to which the contribution of the sensible heat, resulting from the temperature rise, must be deduced from the total heat.

This approach led to the following result:

$$\Delta H_{\text{fusion}} = 130 \text{ kJ kg}^{-1} \pm 3\% \tag{4}$$

This experimental value is in agreement with the data available within the open literature especially with the melting heat of paraffins ranging between 58 and 269 kJ kg^{-1} [18].

3.2. Specific heat of CO_2 adsorption on the RB2 activated carbon

In order to determine the heat of CO_2 adsorption on RB2, a load of 1.654 g of RB2 was introduced into the calorimeter working cell and exposed to successive isothermal CO_2 pressure steps at 30 °C. The obtained calorimetric signals are reported in Fig. 4.

Each pressure step is associated to an exothermic peak. The amount of CO_2 adsorbed at equilibrium for each pressure level was calculated from the adsorption isotherms at

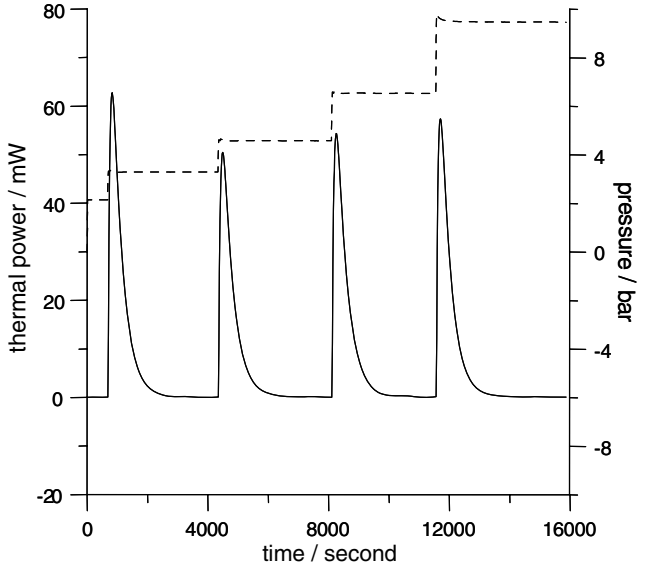

Fig. 4. Heat flow corresponding to successive CO_2 pressure steps, (—) thermal power, (---) pressure.

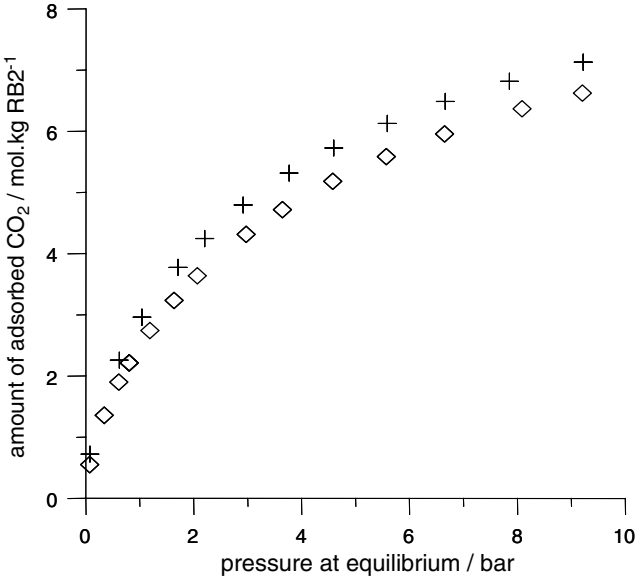

Fig. 5. CO_2 adsorption isotherms at (+) 30 °C and (◇) 40 °C.

30 °C (Fig. 5) determined with a high-pressure volumetric apparatus previously developed in our laboratory.

According to its exothermic character, adsorption led to an increase of the temperature in the working cell. After the thermodynamic equilibrium was reached, the cell was cooled down to 30 °C. The heat of adsorption was calculated using the following equation:

$$\Delta H_{\text{adsorption}} = \frac{\Delta H}{n_{\text{adsorbed CO}_2}} \tag{5}$$

and the following result was obtained

$$\Delta H_{\text{adsorption}} = -511.4 \text{ kJ kg}^{-1} \pm 8\% \tag{6}$$

which is in agreement with the values currently published concerning physical adsorption of carbon dioxide over activated carbons [19].

3.3. Heat capacities of RB2 and adsorbed CO_2

In order to measure the heat capacity of the RB2, a load of 0.763 g was increased in temperature from 24.5 to 34.5 °C at constant heating rate under inert atmosphere (1 bar of nitrogen). The obtained calorimetric signal is reported in Fig. 6.

According to the working conditions, the sole contribution to the calorimetric signal is the RB2 heat capacity which can be calculated as follows:

$$C_{p\text{RB2}} = \frac{W}{m_{\text{RB2}} \frac{\mathrm{d}T}{\mathrm{d}t}}, \tag{7}$$

where W is the heat flow corresponding to the plateau observed between 1000 and 1300 s in Fig. 6, the resulted heat capacity is:

$$C_{p\text{RB2}} = 0.92 \text{ kJ kg}^{-1} \text{ K}^{-1} \pm 5\% \tag{8}$$

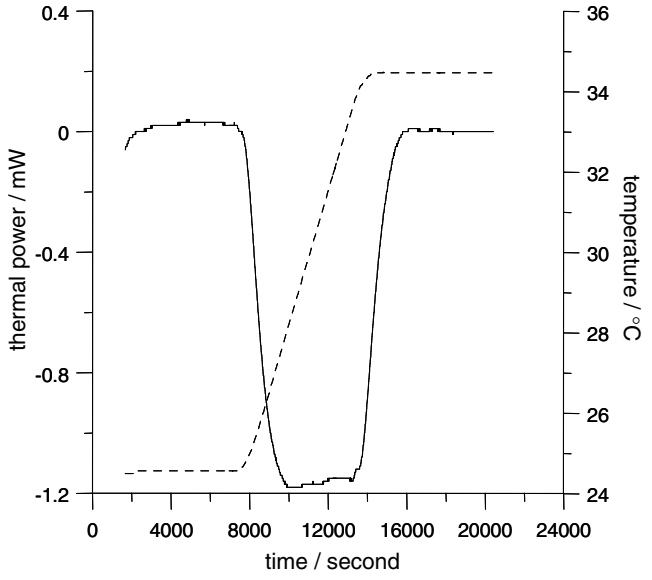

Fig. 6. Heat flow of a sample of RB2 exposed to temperature ramp, (—) thermal power, (----) temperature.

The heat capacity of the adsorbed CO_2 was measured by exposing the RB2 sample under a CO_2 atmosphere. The adsorption/desorption equilibrium is displaced by all temperature change. In order to keep the amount of adsorbed CO_2 roughly constant during the experiments, the pressure was adjusted using the mass flowmeter with respect the appropriate adsorption isotherm. The obtained calorimetric signal of the Fig. 7 showed some irregularities due to the pressure adjustment controlled by the mass flowmeter. Several measurements were carried out under different pressure settings and for various temperature rises. All the experiment led to the following value of the heat capacity of adsorbed CO_2

$$C_{p_{\text{adsorbed CO}_2}} = 1.56\ \text{kJ kg}^{-1}\ \text{K}^{-1} \pm 9\% \quad (9)$$

To our knowledge, only two values are available in the open literature: 1.1 kJ kg K^{-1} [20] and 2.5 kJ kg K^{-1} [21]. The $C_{p\text{adsorbed CO}_2}$ determined in the present study falls within the range of these available values.

3.4. Influence of the PCM on the thermal effects induced by CO_2 adsorption on RB2

Once the thermal characteristics of each component required for the study have been determined, the effect of the μ-PCM on the thermal behaviour of the RB2 during CO_2 adsorption could then be studied. As soon as the CO_2 was introduced into the calorimeter cells, its adsorption induced an increase of the temperature in the working cell. Once the temperature exceeded 35 °C, the PCM was expected to melt, absorb the heat and limit the temperature increase.

The maximum of the peaks obtained when pure RB2 was exposed to different CO_2 pressure steps at 30 °C were plotted versus the corresponding heat generated by adsorption (Fig. 8). This maximum increased linearly and was found to be related to the temperature change of the sample. As the calorimetric apparatus cannot allow a direct measurement of the sample temperature, the peaks heights with and without μ-PCM were considered as the relevant experimental values selected to highlight the μ-PCM efficiency.

3.4.1. PCM effect on the temperature variations of the adsorbent bed

In all the following experiments, the mixture of μ-PCM and RB2 was made of 10% in weight of μ-PCM. The adsorption isotherm of the μ-PCM/RB2 mixture expressed

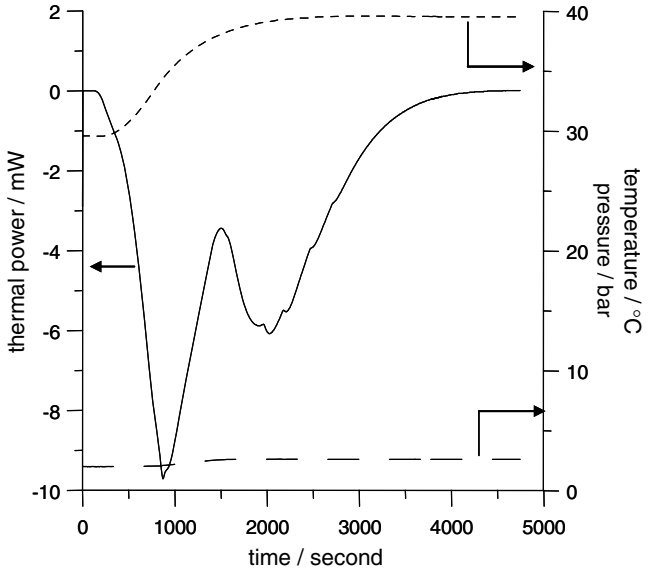

Fig. 7. Heat flow corresponding to RB2 exposed to a temperature rise under CO_2, (—) thermal power, (----) temperature, (——) pressure.

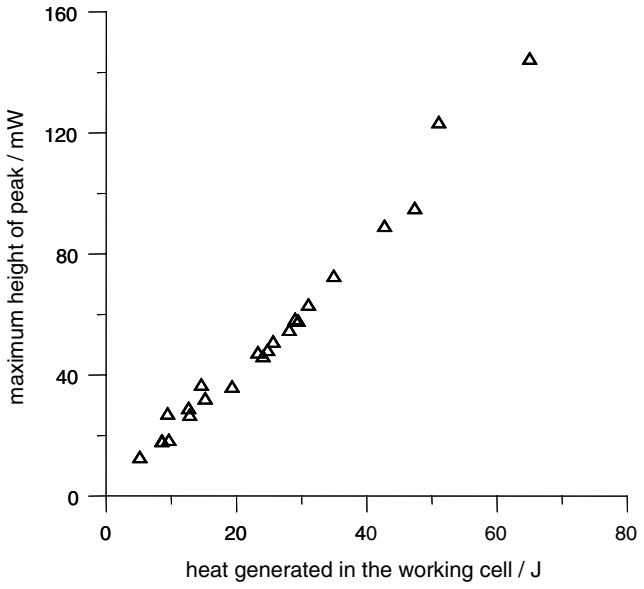

Fig. 8. Relation between peaks height and amount of adsorbed CO_2.

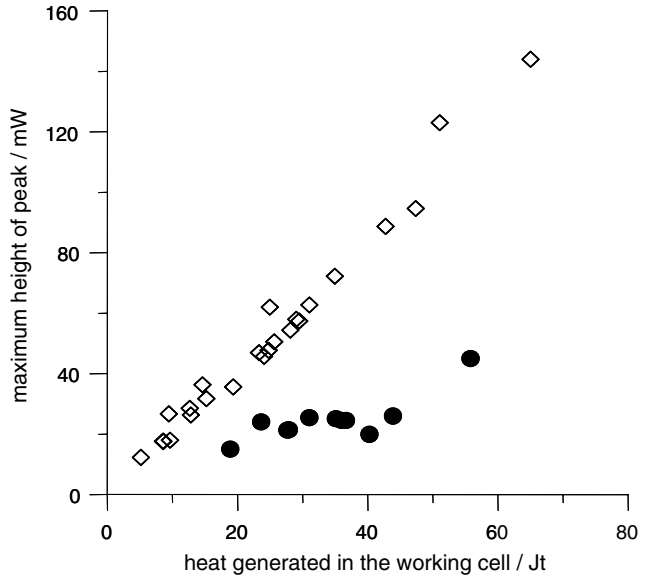

Fig. 9. Comparison of peaks height with during adsorption of CO_2 in RB2 without (◇) and with (●) PCM.

by unit of mass of RB2 should match the isotherm of pure RB2. This has been initially checked using the high pressure volumetric apparatus. It was found that the CO_2 adsorption capacity of the RB2 was not affected by the presence of μ-PCM in the mixture.

Isothermal (30 °C) pressure steps were realized on μ-PCM/RB2 samples of 1.465 g. When a given amount of CO_2 was adsorbed on the RB2, the temperature started to increase in the cell and this initiated the PCM melting. At the adsorption equilibrium, the cell was cooled down to 30 °C and this caused the PCM to solidify again. Then, for a given pressure step, the total energy obtained by the integration of the heat flux was constant during CO_2 adsorption regardless whether RB2 is mixed or not with PCM.

The maxima of the peaks obtained when the composite is exposed to isothermal pressure steps at 30 °C are plotted against the heat released by adsorption in Fig. 9. In the case of μ-PCM/RB2 samples, the maximum of the obtained peaks are lower. Based on this observation, it can be concluded that the PCM decreases the temperature variations inside the working cell during CO_2 adsorption.

The difference between the peaks height obtained with and without PCM increases with respect to the produced heat, this result was predictable. A stronger thermal effect enhances the rather low heat transfer conditions between the μ-PCM and the RB2 and favoured the phase change of the PCM. When the heat induced by adsorption reaches 50 J, the maximum height of the peak starts to increase, probably because the PCM amount is not sufficient to absorb the whole thermal effect.

3.4.2. PCM effect on the apparent specific heat of CO_2 adsorption

The energy balance on the isothermal pressure steps reveals that the PCM does not affect the apparent measured energy. The PCM melts but it solidifies again and the solidifying thermal effect offsets the melting one immediately. As a result, under such working conditions the measured specific heats of CO_2 adsorption are equal with and without PCM.

In order to measure the apparent specific heat of CO_2 adsorption, the PCM has to remain in liquid state after the adsorption process is achieved. To obtain this, the μ-PCM/RB2 mixture was exposed to pressure steps and simultaneous temperature rises. Under these conditions, the PCM would remain liquid after adsorption and its melting would effect the thermal balance.

Using this approach, repeated experiments were conducted and led to similar results. Therefore, only a sole characteristic curve is presented for illustration. Samples of RB2 and μ-PCM/RB2 mixture were exposed to similar experimental conditions i.e., 30–40 °C in temperature range, 1–4.7 bar in pressure range and 5 °C min^{-1} in heating rate. The obtained calorimetric signals are reported in Fig. 10.

The first peak, corresponding to the exothermic CO_2 adsorption effect is lower when PCM is mixed with RB2. Otherwise, the two peaks follow a whole similar behaviour. The second peak, the endothermic one, corresponds to the cumulative effects of the heat capacities of the μ-PCM, the RB2 and the adsorbed CO_2, the desorption of CO_2 due to the temperature rise, and eventually to the melting of the remaining solid PCM. Therefore, this second peak is more pronounced when PCM is mixed to the RB2. According to the fact that the overall heat capacity of the sample mixture is higher and may keep some PCM in solid state, the obtained result was predictable.

In Fig. 10, the peaks boundaries are marked (i) for initial, (inter) for intermediary and (f) for final. At each

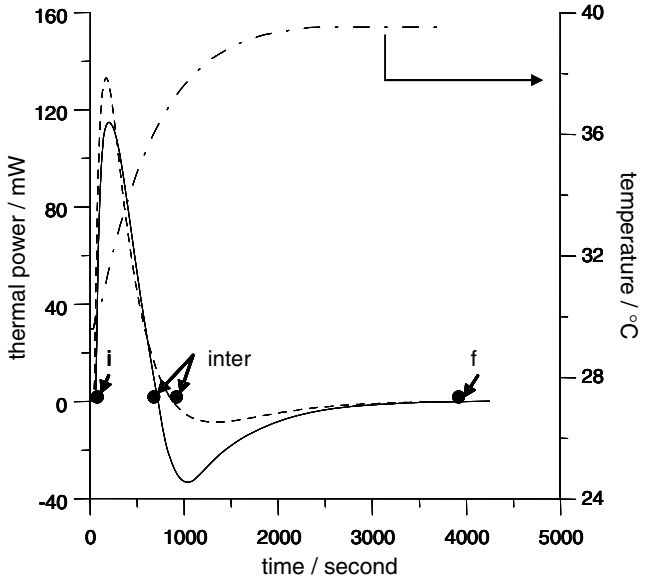

Fig. 10. Heat flow for non isothermal pressure steps, (----) RB2, (—) RB2 with 10% of PCM.

boundary, the temperature and the pressure inside the working cell are known (the temperatures of the working cell and of the calorimeter are equal). Using those working conditions, the adsorption isotherms allow us to determine the amount of adsorbed CO_2 at each boundary n_i, n_{inter}, and n_f.

If the two peaks are considered, the CO_2 adsorption heat can be calculated by the following equation:

$$\Delta H_{adsorption} = \frac{\Delta H_1 + \Delta H_2 - m_{PCM} \cdot \Delta H_{fusion} - C_p \Delta T}{n_f - n_i}, \quad (10)$$

where ΔH_1 and ΔH_2 represent the heat variations calculated by integration of the first and the second peak, respectively, ΔT indicates the temperature variation between the beginning and the end of the experiment and C_p the global heat capacity of the sample.

$$C_p = m_{RB2} \cdot C_{pRB2} + m_{PCM} \cdot C_{pPCM} + m_{adsorbed\ CO_2} \cdot C_{p\,adsorbed\ CO_2} \quad (11)$$

The calculation carried out using the data of Fig. 10 led to the following result:

$$\Delta H_{adsorption} = -514\ kJ\ kg^{-1} \quad (12)$$

This value is in fair agreement with the previous one measured when RB2 was exposed to CO_2.

The integration of the first peak, gives the apparent specific adsorption heat using the Eq. (13). Where ΔT_1 is the temperature change from the beginning to the end of the peak, and $\Delta H_{apparent}$ gives the apparent specific adsorption heat.

$$\Delta H_{apparent} = \frac{\Delta H_1 - C_p \Delta T_1}{n_{inter} - n_i} \quad (13)$$

The efficiency of the PCM with respect to the thermal effect released during adsorption can be calculated as follow:

$$\eta = \frac{\Delta H_{adsorption} - \Delta H_{apparent}}{\Delta H_{adsorption}} \quad (14)$$

From the integration of the second peak, the amount $m_{2melted}$ of PCM that has been melted after adsorption can be calculated:

$$m_{2melted} = \frac{\Delta H_2 - C_p \Delta T_2 - (n_f - n_{inter}) \Delta H_{adsorption}}{\Delta H_{fusion}} \quad (15)$$

As the total amount m_{PCM} of PCM is known, the PCM amount $m_{1melted}$ that has been melted during adsorption can be determined using the following equation:

$$m_{1melted} = m_{PCM} - m_{2melted} \quad (16)$$

For all the experiments carried out on the composite sample, the amount of PCM which was melted during adsorption and the corresponding efficiency have been calculated and reported on Table 1. Moreover, an experiment was carried out between 40 and 50 °C in order to check that when no phase change is involved, the PCM has no effect on the adsorption process.

Table 1
Results obtained from the experiments: pressure step/temperature ramp

Temperature ramp (°C)	Heating rate (°C min^{-1})	Pressure step (bar)	Melted PCM (%)	Efficiency (%)
30–40	10	1–5.2	36	16.3
30–40	5	1–4.7	63.6	23.4
30–40	1	1–4.9	18.2	9.9
30–40	0.1	1–11.3	22.7	14.5
34–36	0.1	1–5.3	100	37.9
34–38	1	1–5.3	90.9	33
40–50	10	1–5.3	0	0

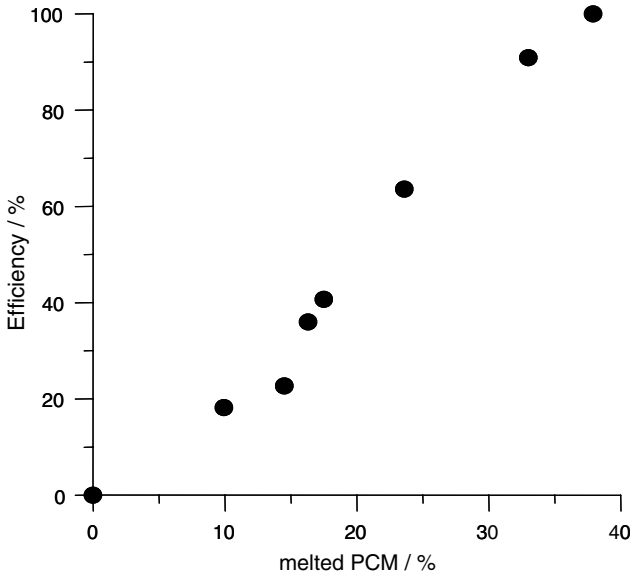

Fig. 11. Relation between the efficiency and the percentage of PCM which was melting during adsorption.

In Fig. 11, the efficiency was plotted versus the percentage of PCM which was melted during adsorption. The gain was found to increases linearly with the amount of molten PCM. Based on this observation, it can be concluded that the melting of the PCM is responsible for the partial consumption of the heat released by the CO_2 adsorption.

When PCM is mixed with the RB2, the temperature variations are decreased as well as the apparent specific heat of CO_2 adsorption. This confirms the effective influence of the PCM on the thermal behaviour of the CO_2 adsorption on RB2.

4. Conclusion

The objective of the whole experimental work was to show the influence of micro-encapsulated PCM material on the thermal behaviour of CO_2 adsorption on activated carbon. Some thermal characteristics of the μ-PCM and the RB2 were required for the general analysis. Consequently, the heat capacities of the μ-PCM, the RB2 and the adsorbed CO_2 were determined as well as the PCM phase change heat and the CO_2 adsorption heat.

The experiments carried out on the μ-PCM/RB2 mixture indicated that in presence of μ-PCM, during adsorption or desorption, the temperature variation inside the adsorbent bed is decreased. The apparent specific heat of adsorption has also been determined and follows the same trend. In term of effective heat of sorption, the μ-PCM efficiency reaches already 33% without any optimisation of the μ-PCM concentration in the composite mixture.

In these experiments the μ-PCM and the RB2 were simply mixed together. Therefore, the heat exchange between the two components could be significantly enhanced by means of a thermal binder. Further works will be done following this approach in order to obtain higher efficiency of the PCM with respect to the apparent heat of sorption. Moreover, the PCM concentration of the mixture has also to be optimized, so all the heat generated by the CO_2 adsorption could be absorbed and the temperature could remain constant during the adsorption and desorption steps.

The resulting materials will be of great interest to control in situ the thermal effects induced in sorption processes in order to enhance their capacities and avoiding hot spots potentially responsible for bed combustion.

Acknowledgements

This work has been done with the financial support of the French Ministry (Program ACI Energie et Conception Durable) and the collaboration from the partners are gratefully acknowledged.

References

[1] K.J. Chang, O. Talu, Behaviour and performance of adsorptive natural gas storage cylinders during discharge, Appl. Therm. Eng. 16 (1996) 359.
[2] V. Goetz, S. Biloe, Efficient dynamic charge and discharge of an adsorbed natural gas storage system, Chem. Eng. Com. 192 (2005) 876–896.
[3] M. Tanczyk, K. Warmuzinski, Multicomponent pressure swing adsorption. Part II Experimental verification of the model, Chem. Eng. Proc. 37 (1998) 301–315.
[4] R.T. Yang, Gas separation by adsorption processes, Butterworth, London, 1986.
[5] W. Lin, S. Farooq, C. Tien, Estimation of overall effective coefficient of heat transfer for nonisothermal fixed bed adsorption, Chem. Eng. Sci. 54 (1999) 4031–4040.
[6] D. Menard, X. Py, N. Mazet, Activated carbon monolith of high thermal conductivity for adsorption processes improvement: Part A: adsorption step, Chem. Eng. Proc. 44 (2005) 1029–1038.
[7] X. Py, V. Goetz, Composite material and use thereof for controlling thermal effects in a physico-chemical process. Int. Patent WO 2004/050789.
[8] C. Chapotard, D. Tondeur, Stockage de chaleur en lit fixe de charbon actif imprégné de paraffine, Entropie (1982) 107–108, 112–121.
[9] G. Nelson, Application of microencapsulation in textile, Int. J. Pharm. 242 (2002) 55–62.
[10] G.L. Nuckols, Analytical modelling of a diver dry suit enhanced with microencapsulated phase change material, Ocean Eng. 26 (1999) 547–564.
[11] D.P. Colvin, G.Y. Bryant, Protective clothing containing encapsulated phase change materials – Advanced in heat and mass transfer in Biotechnology (HTD) New York, ASME 362 (1998) 123–132.
[12] P. Schossig, H.M. Henning, S. Gschwander, T. Haussmann, Micro-encapsulated phase-change materials integrated into construction materials, Solar Energy 89 (2005) 297–306.
[13] S. Gschwander, P. Schossig, H.M. Henning, Micro-encapsulated paraffin in phase-change slurries, Solar Energy 89 (2005) 307–315.
[14] E. Diaz, S. Ordonez, A. Auroux, Comparative study on the gas-phase adsorption of hexane over zeolites by calorimetry and inverse gas chromatography, J. Chromatogr. 1095 (1–2) (2005) 131–137.
[15] Q. Wang, J. Sum, S. Lu, X. Yao, C. Chen, Study on the kinetics properties of lithium hexafluorophosphate thermal decomposition reaction, Solid State Ionics 177 (1–2) (2006) 137–140.
[16] D. Uner, M. Uner, Adsorption calorimetry in supported catalyst charaterization: adsorption structure sensitivity on $Pt/\gamma\text{-}Al_2O_3$, Thermochim. Acta 433 (1–2) (2005) 107–112.
[17] L. Meljac, L. Perrier-Camby, G. Thomas, Calorimetric study of reactions occurring between impregnated activated fibres and hydrogen sulphide, Carbon 43 (7) (2005) 1407–1415.
[18] S. Himram, A. Suwonio, Characterization of alkanes and paraffin waxes for application as phase change energy storage medium, Energy Sources 16 (1994) 117–128.
[19] D.P. Valenzuela, A.L. Myers, Adsorption Equilibrium Data Handbook, Prentice Hall, 1989.
[20] B.K. Sward, M. Douglas LeVan, Examination of the performance of a compression-driven adsorption cooling cycle, Appl. Therm. Eng. 19 (1999) 1–20.
[21] V. Goetz, A. Guillot, An open activated carbon/CO_2 sorption cooling system, Ind. Eng. Chem. 40 (2001) 2904–2913.